Quantification of Path-Integrated Attenuation for X- and C-Band Weather Radar Systems Operating in Mediterranean Heavy Rainfall

GUY DELRIEU

Laboratoire d'Étude des Transferts en Hydrologie et Environnement, Grenoble, France

HERVÉ ANDRIEU

Division Eau, Laboratoire Central des Ponts et Chaussées, Bouguenais, France

JEAN DOMINIQUE CREUTIN

Laboratoire d'Étude des Transferts en Hydrologie et Environnement, Grenoble, France

(Manuscript received 2 April 1999, in final form 20 July 1999)

ABSTRACT

The aim of the current study is to quantify attenuation effects that X- and C-band weather radar systems may experience in heavy rainfall. Part of this information can be obtained from power-law relationships between the attenuation coefficient k (dB km^{-1}) and the rain rate R (mm h^{-1}). These relations exhibit a strong dependence on the wavelength used and a significant influence of the raindrop size and temperature distributions. Here the purpose is to go one step further by providing estimates of the path-integrated attenuations (PIAs) that could be observed as a function of range for a given wavelength. Obviously, these values depend on the space and time structure of rainfall and, therefore, refer to a given climatological context. The methodology used consists of using k–R relations to downgrade carefully processed S-band radar data to the corresponding X- and C-band signals. The data were collected in the Cévennes region, a Mediterranean region in France subject to intense and long-lasting rain events during the autumn season. A refined data processing procedure was applied to the available reflectivity measurements, including ground-clutter removal and correction for the effects of the vertical profile of reflectivity as well as a final bias adjustment using rain gauge data. For three rain events, 75 h of instantaneous rain-rate fields thus were available with total rain amounts that exceeded 300 mm over most of the area of interest. Examples of attenuated profiles are presented, and PIA-range-frequency curves are established for the two wavelengths considered under various hypotheses that concern the raindrop size distribution. One of the results is that, at C band, a PIA of 3 dB is exceeded for 5% of the rain-rate profiles at a range of 50 km. Another finding is that a multiplicative factor of about 6 exists between C- and X-band attenuation effects. Implications for rain-rate estimation at X- and C band are discussed.

1. Introduction

In most of the textbooks (e.g., Collier 1989; Doviak and Zrnić 1993; Sauvageot 1992) and review papers (e.g., Smith 1986; Joss and Waldvogel 1990) devoted to weather radar applications in meteorology and hydrology, the choice of the operating wavelength is presented as an important and difficult compromise. The traditional candidates are the S-band (10 cm) and the C-band (5 cm) wavelengths, even if some systems operating at shorter wavelengths [X- (3.2 cm), Ka- (1.15 cm), and K band (0.86 cm)] have been used in spaceborne and airborne configurations [see Hildebrand and Moore (1990) for a review]. The X band also has been considered recently for ground-based weather radar applications in urban and mountain hydrology (Delrieu et al. 1997). The definite advantage of the 10-cm wavelength over the shorter wavelengths is that it is almost immune to attenuation by rainfall. This advantage comes at a high price, however, because the antennas of 10-cm radars have to be much larger, and their transmitted powers much higher, to retain a reasonable resolution and sensitivity.

The aim of the current paper is a quantification of the attenuation effects that ground-based weather radars may experience in Mediterranean heavy rainfall. This study is based on the dataset collected during the Cévennes 1986–88 Hydrometeorological Experiment (Andrieu et al. 1997; Creutin et al. 1997). The Cévennes region (southern part of the French Massif Central; Fig.

Corresponding author address: Dr. Guy Delrieu, LTHE, UMR 5564 (CNRS, UJF, INPG, IRD), BP53, F-38041 Grenoble, Cedex 9, France.
E-mail: guy.delrieu@hmg.inpg.fr

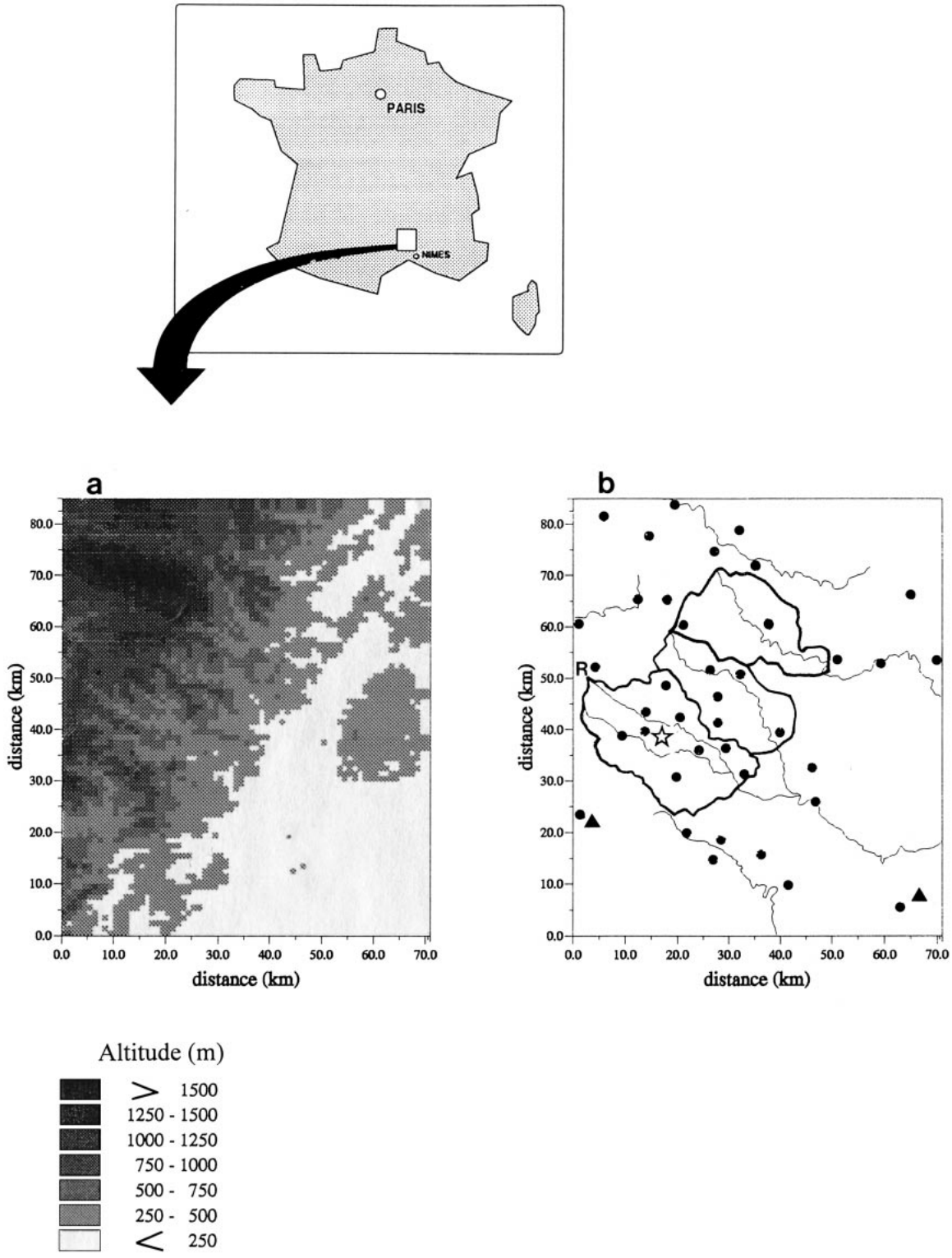

FIG. 1. Presentation of the study area. (a) The digitized terrain model of the Cévennes region is displayed together with (b) the locations of the rain measurement devices (letter R for the ANATOL radar, black circles for the rain gauges, and a star for the disdrometer) and the delineation of some of the hydrologically sensitive watersheds of the region.

1) is prone to severe and long-lasting rainfall events, mainly during the autumn season, that are widespread geographically and can cause flash floods. In section 2 a procedure aimed at establishing the relationships between the rain rate R (mm h^{-1}) and the radar measurables, that is the equivalent radar reflectivity factor Z_e (mm^6 m^{-3}) and the attenuation coefficient k (dB km^{-1}), is presented. The procedure is based on drop size distribution (DSD) measurements performed at ground level with a Joss–Waldvogel disdrometer. The diffusion and absorption of the electromagnetic waves by the hydrometeors are described using the Mie theory. Both the k–R and the Z_e–R relations are assumed to be represented with sufficient accuracy by means of the classical power-law model as follows:

$$k = cR^d \quad \text{and} \tag{1}$$

$$Z_e = aR^b, \tag{2}$$

To expand the characterization of attenuation effects for the attenuated wavelengths that could be used for hydrometeorological surveillance (C-, X band) in such regions, we propose to account for the space–time distribution of rain in order to estimate the probability distribution of path-integrated attenuations (PIA) as a function of range. Note that, although the applications are different, this problem is classical for earth and terrestrial communication engineers (e.g., Boithias 1984). Knowing the rain-rate profile $R(r)$ in a given horizontal direction s in space, a straightforward estimation of PIA (dB) at a given range r is given by

$$\mathrm{PIA}(r) = 2c \int_0^r R(s)^d \, ds. \tag{3}$$

Based on Weible and Sirmans (1976), the main assumption in the current work is that the required rain-rate fields can be derived from carefully processed S-band radar data. Because it is a critical point for the current study, the processing of the so-called ANATOL radar dataset used herein is recalled briefly in section 3. An extensive description of the Cévennes 1986–88 experiment can be found in Andrieu et al. (1997) and Creutin et al. (1997). In section 4, the PIA simulation is illustrated for various rain-rate profiles. This description is followed by a discussion of the results obtained in terms of PIA distribution functions calculated over the available sample for the two wavelengths considered.

2. DSD and (Z_e, k, R) relationships

A straightforward approach is considered for the establishment of the (Z_e, k, R) relationships (Delrieu et al 1991, 1999a). The classical exponential model for the DSD originally proposed by Marshall and Palmer (1948) is considered first:

$$N(D, R) = N_0 \exp[-\Lambda(R)D], \tag{4}$$

where the N_0 parameter usually is assumed to be constant, and the parameter Λ is expressed as a power-law model of the rain rate R,

$$\Lambda(R) = \Lambda_1 R^{\Lambda_2}. \tag{5}$$

After Bennett et al. (1984), a particularity of the current approach lies in the fact that the three DSD parameters (N_0, Λ_1, Λ_2) are constrained so that the rain-rate integral equation is satisfied:

$$R = 0.6 \times 10^6 \Pi \int_{D_{\min}}^{D_{\max}} N(D, R) v_t(D) D^3 \, dD, \tag{6}$$

where $v_f(D)$ is the terminal velocity of raindrops of diameter D, and ($D_{\min}$, $D_{\max}$) is the range of drop diameters. The numerical factor in front of the integral holds if R is in millimeters per hour, $v_t(D)$ is in meters per second, $N(D, R)\,dD$ is in 1/(cubic centimeters), and D is in centimeters. To satisfy this constraint, Λ_1 and Λ_2 are fitted using DSD measurements averaged into rain-rate classes, and a normalized N_0 parameter, denoted N_0', is calculated as

$$N_0'(R) = \frac{R}{0.6 \times 10^6 \Pi \displaystyle\int_{D_{\min}}^{D_{\max}} \exp[-\Lambda(R)D] v_t(D) D^3 \, dD}. \tag{7}$$

Figure 2 presents the adjustments obtained for the Cévennes DSD data using the proposed procedure. Note that rain rates of up to 90 mm h^{-1}, during the 1-min integration time step considered, are observed in this dataset. A well-known characteristic of the exponential model is that it overestimates the disdrometer DSD measurements for diameters of less than 0.2 cm. Delrieu et al. (1991) also adjusted a gamma model to this dataset. The effect of this model choice was found to be small in terms of the resulting k–R relationships in comparison with the effects of temperature and DSD type. Table 1 gathers the parameters of the corresponding DSD model as well as two other models proposed elsewhere in the literature. The so-called widespread and thunderstorm DSD models are derived from the Marshall and Palmer (1948) and the Joss and Waldvogel (1969) models by applying the N_0 normalization. Practical implementation of the method shows that N_0' slightly depends on the rain rate. The last column of Table 1 gives the resulting N_0'–R power-law models. The terminal velocities derived from Beard's model (Beard 1976) are considered in this calculation. Note that the Cévennes DSD model falls between the widespread and thunderstorm models, a result consistent with the meteorological nature of the Cévennes rain events.

With knowledge of the DSD model, Z_e (mm^6 m^{-3}) and k (dB km^{-1}) are calculated using the following equations

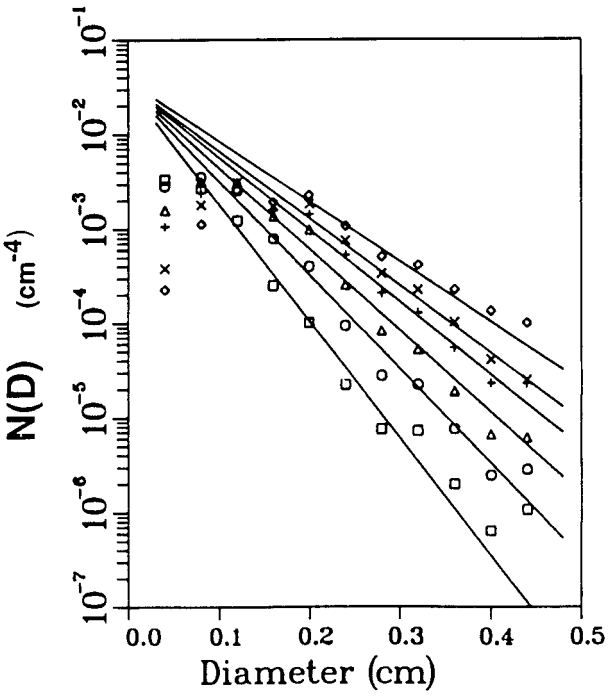

FIG. 2. Cévennes mean disdrometer DSDs for rain-rate classes of 1–5 (square), 5–10 (circle), 10–20 (triangle), 20–30 (plus sign), 30–40 (cross), and greater than 40 mm h^{-1} (diamond). The fittings provided by the exponential model according to the procedure described in section 2 are given by the continuous lines. Values of the corresponding parameters can be found in Table 1. For clarity in plotting, experimental DSDs were aggregated into classes 0.04 cm in width (the original disdrometer diameter class is 0.02 cm).

$$Z_e(R) = 10^{12}\frac{\lambda^4}{\Pi^5|K|^2}\int_{D_{\min}}^{D_{\max}} N(D, R)\sigma_b(D)\, dD, \qquad (8)$$

and

$$k(R) = 0.4343 \times 10^6 \int_{D_{\min}}^{D_{\max}} N(D, R)Q_t(D)\, dD, \qquad (9)$$

where λ is the wavelength (expressed here in centimeters); $\sigma_b(D)$ and $Q_t(D)$ are the Mie backscattering and total attenuation cross sections (square centimeters), respectively, of a raindrop supposed to be spherical with diameter D. Note that the Mie theory is preferred in the current case because the Rayleigh approximation is known to be unacceptable for attenuation and not fully satisfactory for backscattering for wavelengths that are less than or equal to 3.2 cm. The constant $|K|^2$ depends on the complex refractive index of the hydrometeor. The term "equivalent," associated with Z_e, is related to the fact that a value of about 0.93, valid for water, has been used for $|K|^2$ in (8). The $(D_{\min}, D_{\max})$ diameter range considered in Eqs. (8) and (9) was chosen to be (0, 0.6 cm), a reasonable extension when compared with the disdrometer diameter range of (0.02, 0.52 cm), even though some authors suggest that a maximum diameter of 10 mm should be accounted for in such calculations (Smyth and Illingworth 1997). A partial assessment of the DSD model truncation can be found in Delrieu et al. (1991) with a modest effect on the k–R relationship. Of course, a much higher effect is expected on the Z_e–R relationship that, however, is of lesser concern for the current study.

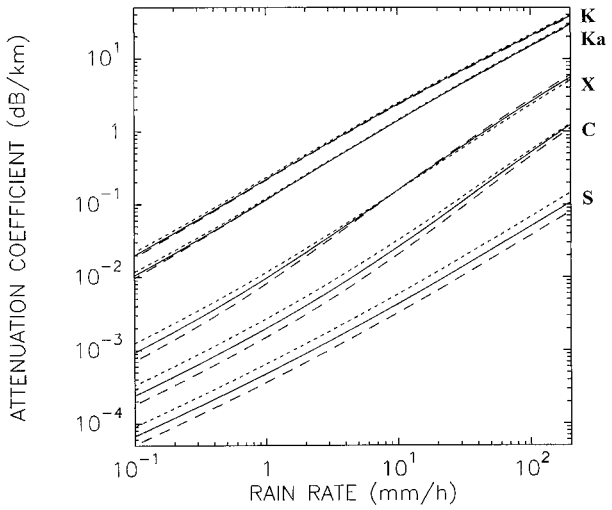

FIG. 3. Some examples of k–R relationships established using Mie theory (spherical rain drops) for the K- (0.86 cm), Ka- (1.15 cm), X- (3.2 cm), C- (5.6 cm), and S-band (10 cm) wavelengths and the Cévennes DSD model (see Table 1) for raindrop temperatures T = 0°C (dotted line), T = 10°C (continuous line), and T = 20°C (dashed line).

Examples of k–R curves resulting from Eq. (9) are displayed in Fig. 3 for the Cévennes DSD data, raindrop temperatures of 0°, 10°, and 20°C and wavelengths of 0.86, 1.15, 3.2, 5.6, and 10 cm. The well-known wavelength dependence of these curves clearly appears; note that the X-band attenuation coefficients are 5 to 7 times bigger than the C-band coefficients. Furthermore, the influence of the raindrop temperature remains limited

TABLE 1. Parameters of some exponential DSD models proposed in the literature. The variable $N'_0(R)$ is a normalized value of the parameter N_0, which guarantees the consistency of the DSD model with respect to the rain-rate integral equation.

DSD model name	Reference	$\Lambda(R)$ (cm^{-1})	N_0 (cm^{-4})	N'_0 (cm^{-4})
"widespread"	Marshall and Palmer (1948)	$41.0R^{-0.21}$	0.08	$0.0626R^{0.033}$
	Joss and Waldvogel (1969)		0.07	
"Cévennes"	Delrieu et al. (1991)	$35.0R^{-0.215}$	–	$0.0310R^{0.025}$
"thunderstorm"	Joss and Waldvogel (1969)	$30.0R^{-0.21}$	0.014	$0.0141R^{0.059}$

TABLE 2. Coefficients of the k–R (c, d) and the Z_e–R (a, b) power-law relationships for the 3.2- and 5.6-cm wavelengths, the DSD exponential models presented in Table 1, and raindrop temperatures T of 0°, 10°, and 20°C (R: mm h^{-1}, k: dB km^{-1}, and Z_e: mm^6 m^{-3}).

DSD model name	T (°C)	c, d, a, b (X band)	c, d, a, b (C band)
"widespread"	0	9.12×10^{-3}, 1.17, 221, 1.56	1.91×10^{-3}, 1.17, 241, 1.44
	10	7.43×10^{-3}, 1.23, 204, 1.59	1.30×10^{-3}, 1.23, 242, 1.43
	20	6.13×10^{-3}, 1.29, 189, 1.62	9.24×10^{-4}, 1.26, 247, 1.40
"Cévennes"	0	1.02×10^{-2}, 1.18, 380, 1.53	1.90×10^{-3}, 1.23, 366, 1.42
	10	9.20×10^{-3}, 1.22, 363, 1.56	1.32×10^{-3}, 1.29, 362, 1.40
	20	8.37×10^{-3}, 1.26, 353, 1.58	9.43×10^{-4}, 1.34, 367, 1.38
"thunderstorm"	0	1.20×10^{-2}, 1.16, 650, 1.46	2.13×10^{-3}, 1.24, 550, 1.37
	10	1.16×10^{-2}, 1.19, 646, 1.48	1.55×10^{-3}, 1.30, 533, 1.36
	20	1.13×10^{-2}, 1.22, 653, 1.49	1.14×10^{-3}, 1.34, 530, 1.33

for the wavelengths less than or equal to 3.2 cm and is more pronounced for the S- and C bands. Because of the poor log–log linearity of these curves, the power-law relationships were adjusted over a limited range of rain-rate values (1–100 mm h^{-1}). The resulting coefficients (c, d) are presented in Table 2, together with the corresponding Z_e–R power-law model coefficients (a, b) for the X- and C bands, the Cévennes, widespread and thunderstorm DSD models, and temperatures of 0°, 10°, and 20°C.

3. Rain-rate fields

One of the aims of the Cévennes 1986–88 experiment was to test an S-band weather radar system for the hydrological application in this mountainous area (Fig. 1). The mobile ANATOL radar was set up near Barre des Cévennes at an altitude of 1030 m above mean sea level (MSL). The main characteristics of this radar are a 3-dB beamwidth of 1.8°, a peak power of 250 kW, a pulse length of 2 m s^{-1}, and a minimum detectable signal of 22 dBZ at 100 km. Because of the topography of the region, a good radar coverage thus was obtained for an area of about 5000 km^2, including the most sensitive watersheds of the region from a hydrological point of view (Gardons d'Anduze, d'Alès, Cèze, etc.). Hourly accumulations from 41 rain gauges were available for radar data calibration and validation purposes. As an illustration of the magnitude of these rain events, Table 3 presents the characteristics of the rain gauge data collected during the three major events observed during the experiment, namely the events that occurred on 13–15 November 1986, 4–6 October 1987, and 11 October 1988. Note that total rain amounts exceeding 300 mm in 75 h are observed over most of the study area during the selected periods.

TABLE 3. Some rain gauge values recorded during the three major rain events of the Cévennes 1986–88 experiment.

Date	Maximum total rain amount over the rain gauge network (mm)	Maximum hourly rain amount over the rain gauge network (mm)	Duration* (h)
13–15 Nov 1986	512	33	48 (38)
4–6 Oct 1987	370	60	40 (32)
11 Oct 1988	337	225 (in 2 h)	20 (5)

* In parentheses, the duration of the records effectively accounted for in the PIA simulation is given.

The radar was operated using a two-elevation scan strategy with elevation angles of about 1.0° and 3.0°. The following processing steps were applied to the data.

a. Identification and correction of the vertical profile of reflectivity (VPR)

One of the major sources of error in mountainous regions is related to the vertical variations of the reflectivity within and below the radar resolution volume. This fact is true especially in the current case because of the altitude of the radar site. The radar beam more frequently crosses the 0°C freezing level, causing increased brightband effects, and overshoots cloud tops, with the associated partial beam-filling effects. An extensive amount of work has been devoted to this question using the Cévennes dataset (Andrieu and Creutin 1995; Andrieu et al. 1995, 1997; Creutin et al. 1997) and interested readers are referred to these papers for a detailed consideration of this problem. Reported here are the general ideas behind this work and the expected influence of VPR in the considered measurement configuration. The basic assumption is to consider that $Z_e(r, h)$ at a given r and a given altitude h may be broken into two independent terms:

$$Z_e(r, h) = Z_e^0(r)z(h), \tag{10}$$

where $Z_e^0(r)$ represents the horizontal variations of the reflectivity factor at a given reference level h_0, and $z(h)$, the so-called VPR, represents the variations of the reflectivity factor as a function of the altitude, assumed to be independent of range. Introduction of this formalism in the weather radar equation (Doviak and Zrnić 1993; Andrieu et al. 1997) yields for the measured reflectivity factor $Z_m(r, s)$ at a given elevation angle s an expression of the following type:

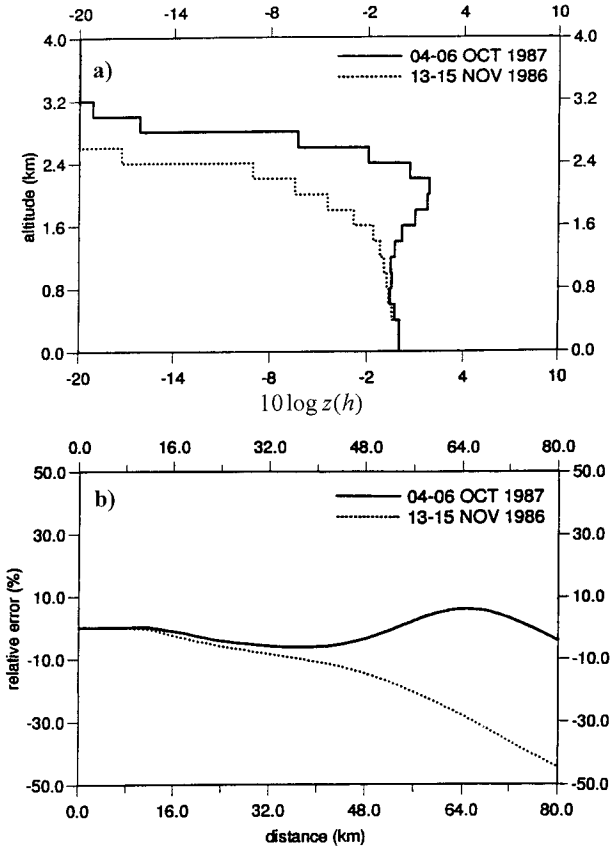

FIG. 4. (a) Mean vertical profiles of reflectivity observed during two rain events of the Cévennes 1986–88 experiment. Note that the altitude scale refers to the radar altitude h_0 equal to 1030 m. As an illustration of the VPR influence in the current context, (b) presents the evolution of the resulting relative error RE (%) on the rain rate as a function of range for an elevation angle of 1° and a 3-dB beamwidth of 1.8°.

$$Z_m(r, s) = Z_e^0(r) z_a(r, s), \tag{11}$$

with

$$z_a(r, s) = \iiint_{V(r)} f^4(\theta, \psi) z(h)\, dV. \tag{12}$$

The so-called *apparent* VPR $z_a(r, s)$ is the integral of VPR over the radar resolution volume $V(r)$ weighted by the power distribution over the radar beam axis [$f^4(\theta, \psi)$ in Eqn. (12) denotes the two-way antenna diagram]. An inverse method was proposed to identify the VPR, given 1) the characteristics of the radar beam and 2) the curves of the ratio $q_m(r)$ of measured reflectivities at (at least) two elevations. The $q_m(r)$ variable is interesting because it allows one to filter the horizontal variations of the reflectivity $Z_e^0(r)$ if the decomposition given by Eqn. (11) holds. Figure 4a displays the mean VPR resulting from the proposed identification procedure for two rain events (13–15 November 1986 and 4–6 October 1987), the altitude of the radar (1030 m MSL) being the reference level h_0. Note that 1) the study area chosen for the VPR identification covers the azimuth sector between N60° and N170° for ranges less than 65 km and 2) VPR is assumed to be constant within the geographical domain where the analysis is performed. For both rain events, the maximum altitude of the reflectivity falls between 3000 and 4000 m MSL. A significant brightband effect is visible on the mean VPR for the 4–6 October 1987 rain event. As an illustration of the expected influence of VPR in the considered context, Fig. 4b presents the resulting relative error RE on the rain rate at ground level for measurements realized at an elevation of 1°. Note that RE is given by

$$\mathrm{RE}(r, h) = z_a(r, h)^{1/b} - 1. \tag{13}$$

Figure 4b clearly shows the very significant rain underestimation for ranges greater than 40 km for the 13–15 November 1986 rain event. For the 4–6 October 1987 rain event, the brightband effect partly compensates for the partial beam filling effect for ranges between 40 and 70 km. The identification method also was applied at an hourly time step to determine the time variability of VPR within the rain event; it was shown that almost one-half of the hourly VPRs for this event do not exhibit a brightband effect (Andrieu et al. 1997). Therefore the mean VPR displayed in Fig. 4a is thought to be too optimistic in terms of the RE criterion. Note that these *hourly* VPRs were taken into account in the current study to estimate the instantaneous reflectivity fields at the reference level from reflectivity measurements aloft.

b. Corrections of ground clutter and beam blockage

Simple rules were applied to obtain composite reflectivity data from the two available elevation angles. The driving idea was to favor the lowest elevation angle to obtain measurements as representative as possible of rainfall reaching the ground. The data of the upper elevation angle were used only when the low–elevation angle data (1) were affected by ground clutter or (2) required too high a beam-blockage correction factor. An interpolation scheme based on surrounding pixels was used if the upper elevation angle measurement also was unusable. Note that, in the simulation of attenuation effects proposed in section 4, the azimuth sector was chosen so as to exclude the main regions subject to ground clutter and beam blockage (Mont Lozère: N0° to N60°; Mont Aigoual: N170° to N180°).

c. Bias adjustment

In addition to the processing of the VPR- and relief-induced errors (note that these corrections are based on radar data only), a bias correction was applied by means of a factor, supposed to be constant in time and space for a given rain event, derived from a global radar–rain gauge comparison. This correction aims at compensating a radar miscalibration and/or the effects of an ill-

adapted Z_e–R relationship. The results of the hydrological validation (Creutin et al. 1997) support the major assumption of the current work, namely, that the available carefully processed radar data provide realistic instantaneous rain-rate profiles within 60 km from the radar at the reference level h_0.

4. Simulation of attenuation effects

In this section, the reference rain-rate fields derived from the S-band radar data according to the procedure described in section 3 are used together with the k–R relationships derived in section 2 to estimate PIAs for the two wavelengths considered using Eqn. (3). Because hydrologists are not familiar with PIAs, it is worth mentioning here the relation that exists between PIA and the ratio of the attenuated (R_a) to the nonattenuated (R) rain rates derived from radar reflectivity measurements at a given range r, namely,

$$R_a(r)/R(r) = 10^{-\mathrm{PIA}(r)/10b}, \qquad (14)$$

where b is the exponent of the corresponding Z_e–R relationship (see Table 2). As a quantitative example, for $b = 1.5$, Eqn. (14) yields R_a/R ratios of 0.631, 0.215, and 0.046 for PIAs of 3, 10, and 20 dB, respectively.

Figures 5–7 provide three examples of attenuated rain-rate profiles. In each figure, the top graph presents a typical rain field observed during the Cévennes 1986–88 experiment. The middle graph displays the rain-rate profile observed in the azimuth direction indicated in the top image, together with the profiles that would have been obtained with a C- or an X-band radar according to the hypotheses described above. The bottom graph shows correspondingly how PIA builds up as a function of range for the two wavelengths considered.

Figure 5 corresponds to a very active cold front, a frequent situation resulting from the conflict of polar air coming in from the northwest with hot and humid air advected from the Mediterranean Sea. For the rain-rate profile observed in the azimuth direction 126° (triangular shape, depth of 10 km, peak value of about 120 mm h^{-1}), the X-band (C-band) PIA over the entire profile is equal to 28.5 dB (5.4 dB), and the peak rain rate is underestimated by a factor of 12 (1.67) if the Cévennes DSD and a temperature of 10°C are used to derive the (c, d) coefficients required in Eqn. (3). Figure 6 presents the case of a widespread rain field more typical of the warm sector of Mediterranean perturbations. The profile extracted in the azimuth direction 129° reaches locally a maximum value of about 50 mm h^{-1} and presents rain rates exceeding 10 mm h^{-1} over about 60 km in range. In that case, PIAs over the entire profile reach values of 52.6 and 9.3 dB for the X- and C bands, respectively. Last, Fig. 7 gives the case of very intense rain convective cells having a size of a few kilometers that cross the area of interest from south to north at a speed close to 60 km h^{-1}. For the azimuth direction 81°, two such rain cells are aligned, resulting in PIAs of 45.8

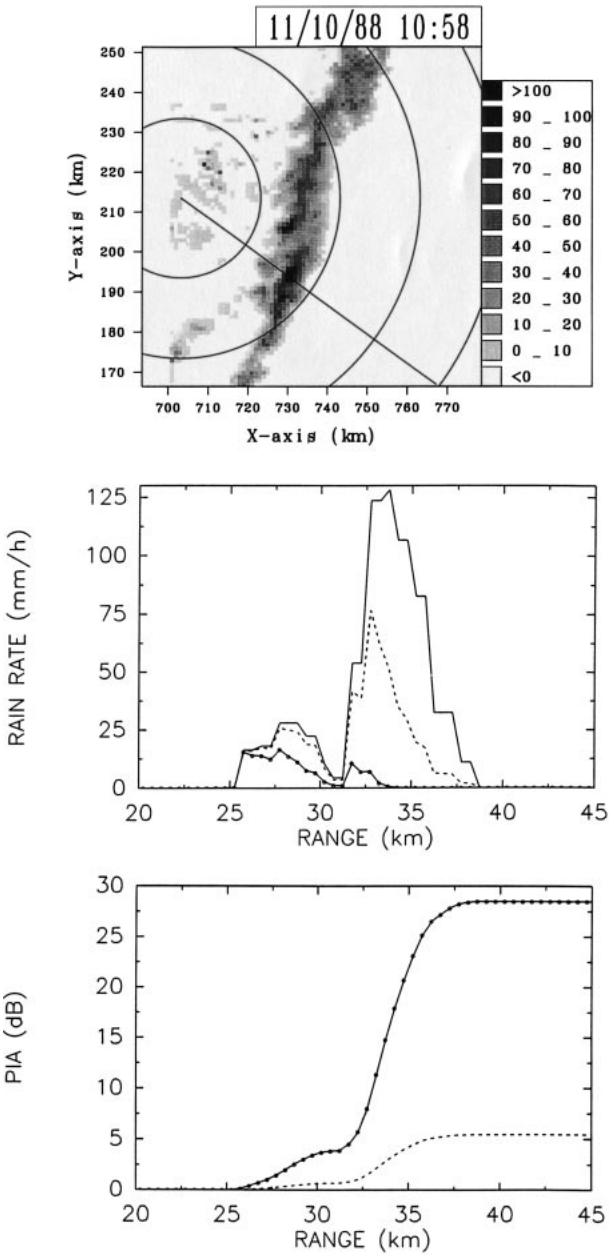

FIG. 5. Illustration of the simulation procedure for a very active frontal rainfield observed during the Cévennes 1986–88 experiment on 11 Oct 1988 at 1058 LST. The top graph presents the spatial distribution of the rain rates (mm h^{-1}) derived from the S-band radar data according to the procedure described in section 3. The middle graph shows the rain-rate profiles corresponding to the azimuth direction indicated on the top graph. The continuous line represents the observed rain-rate profile, and the dotted line and the line with circle markers correspond to attenuated rain-rate profiles at the C- and X bands, respectively. The k–R relationships derived from the Cévennes DSD model and $T = 10$°C are considered in the calculation (Table 2). The bottom graph shows the corresponding PIA as a function of range.

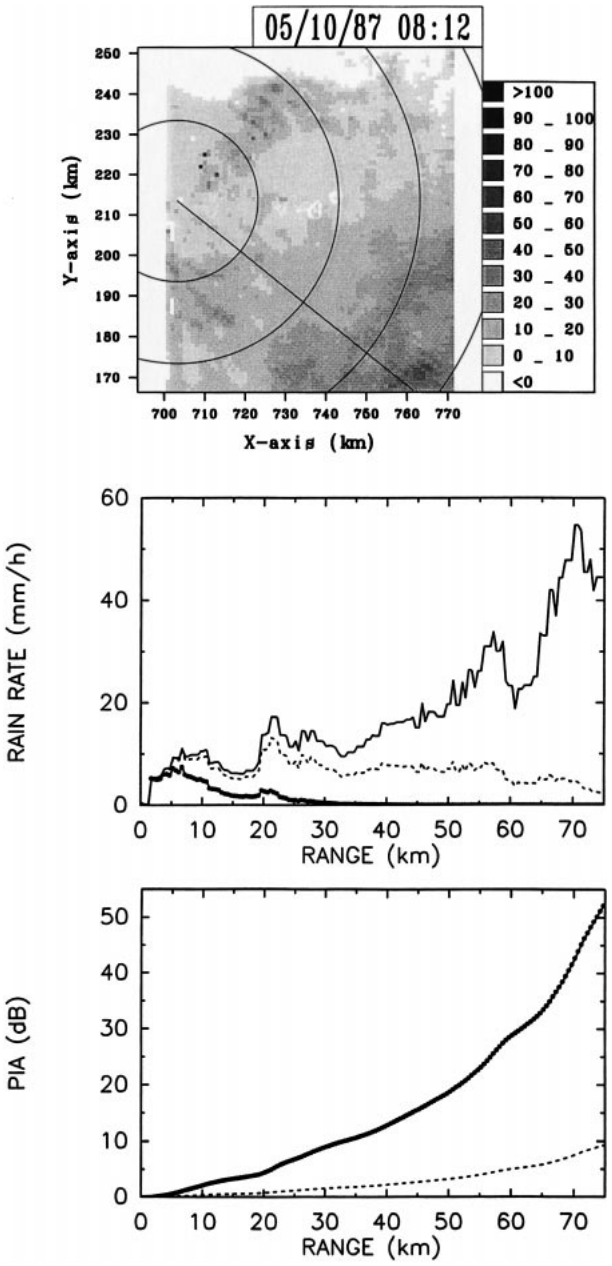

FIG. 6. Same as Fig. 5 for a widespread rain field observed during the Cévennes 1986–88 experiment on 5 Oct 1987 at 0812 LST.

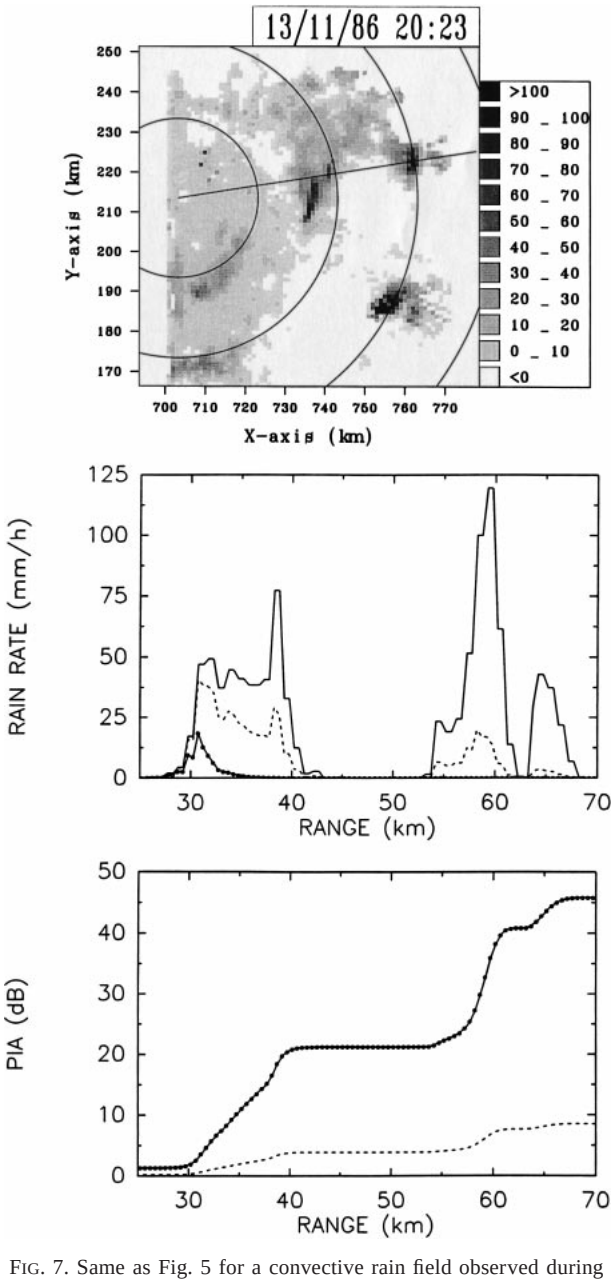

FIG. 7. Same as Fig. 5 for a convective rain field observed during the Cévennes 1986–88 experiment on 13 Nov 1986 at 2023 LST.

and 8.5 dB over the entire profile for the X- and C bands, respectively.

Figures 8–10 aim at answering the following question: how frequently do the very impressive distortions of the rain-rate profiles presented in Figs. 5–7 occur? The simulation procedure was applied to 9600 rain-rate profiles observed during the 75 h of available data in the azimuth range of 60°–150°. An azimuth increment of 5° was considered, that is, 19 rain-rate profiles (in the original polar form of the measured reflectivity data) were extracted from each radar image in the sector for which the confidence in the radar estimates was maximum. The PIAs were calculated and the corresponding cumulative frequency curves established for various ranges between 2 and 60 km. The Cévennes k–R relations (temperature $T = 10$°C), thought to be the most representative in the current context, were used in the simulation as were the widespread ($T = 20$°C) and the thunderstorm ($T = 0$°C) relations to assess the variations of the statistics with DSD and raindrop temperature. Indeed, these two relations give the minimum and maximum attenuation coefficients, respectively, for the range of DSD and temperature considered here. Figure

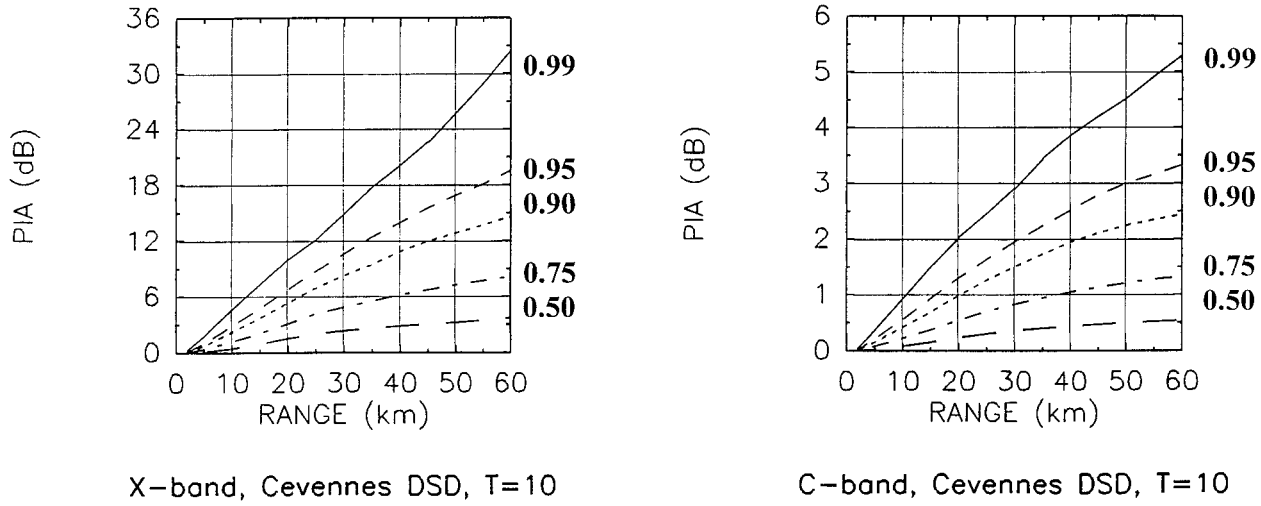

FIG. 8. PIA-range-frequency curves for the (left column) X-band and (right column) C-band wavelengths for the Cévennes k–R relationship ($T = 10$°C). The solid line joins the 0.99 quantiles of the PIA empirical cumulative distribution functions calculated at several ranges. Other lines correspond to the 0.95 (dashed line), 0.90 (dotted line), 0.75 (dash-dotted line), and 0.50 (that is, the median; long-dashed line) quantiles. Example: for the C band, a two-way PIA of 3 dB is not exceeded at a range of 50 km for 95% of the rain-rate profiles.

8 yields, for instance, that, for the C band, the percentage of PIAs exceeding 3 dB at a range of 50 km is equal to 5% if one assumes the Cévennes k–R relation describes attenuation effects satisfactorily. For the same wavelength, range, and quantile, this PIA value varies between 2 (widespread DSD; $T = 20$°C; Fig. 9) and 4.2 dB (thunderstorm DSD; $T = 0$°C; Fig. 10). Note that a factor of 6 was accounted for in the scale of the axes of the X-band PIAs with respect to the C-band PIAs. This factor scales the frequency curves for the Cévennes DSD remarkably well for all ranges (Fig. 8). This value therefore should be kept in mind as a multiplicative factor existing between C- and X-band attenuation effects in this climatological context. Note also that the equifrequency curves present a significant curvature. This fact denotes an inhomogeneity of the rain fields over the measurement area, with higher attenuation effects in the midranges (20–40 km). This feature is not unrealistic if one refers to the rain climate description of the region (Tourasse 1981).

5. Conclusions

This paper aimed at quantifying attenuation effects that X- and C-band weather radars may experience in heavy rainfall typical of the Mediterranean region. From the methodological point of view, the validity of the results obtained relies on the assumption of the representativeness of both 1) the instantaneous rain-rate fields derived from carefully processed S-band radar data and

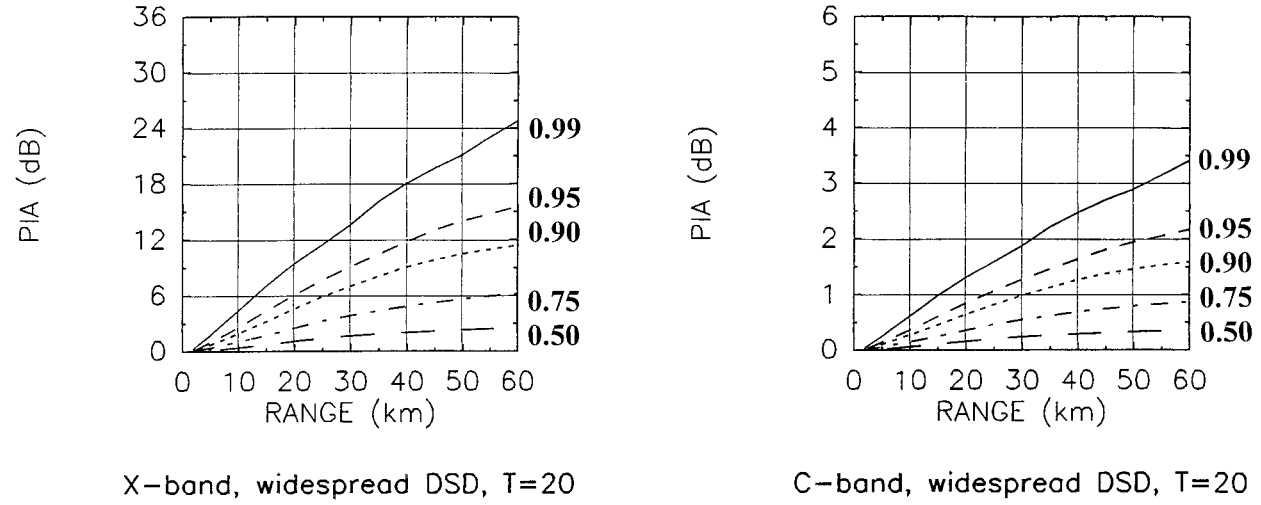

FIG. 9. Same as Fig. 8 for the widespread k–R relationship ($T = 20$°C).

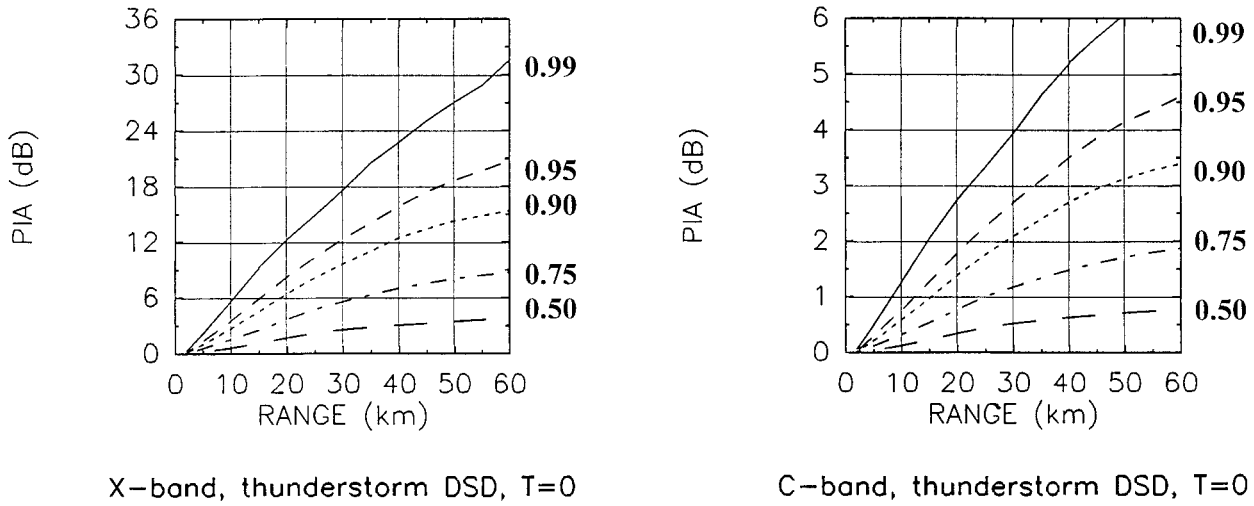

FIG. 10. Same as Fig. 8 for the thunderstorm *k–R* relationship ($T = 0°C$).

2) the *k–R* relationships used to convert rain rates into attenuation coefficients all along the profiles. In this respect, the VPR correction applied to the measured reflectivity data is thought to be of prime importance in the current study because it certainly produces homogenization of the rain-rate profiles with respect to the variations of the DSD with the altitude. The bias adjustment and the hydrological validation based on radar–rain gauge comparison (Creutin et al. 1997) provide additional guarantees concerning the representativeness of the rain-rate profiles. The use of various *k–R* relationships also allowed partial assessment of the influence of the DSD variations. From the practical point of view, Figs. 5–7 clearly show the importance of the problem in terms of rain-rate estimation for both wavelengths, and Figs. 8–10 provide PIA statistics at various ranges based on 75 h of intense Cévennes rainfall. The information contained in these figures needs to be related to the possibilities existing for correcting attenuation effects. Delrieu et al. (1999a) have studied the sensitivity of the attenuation equation with respect to the wavelength, raindrop size distribution, and radar calibration. They showed that, because of the inherent instability of the analytical solution of the attenuation equation first derived by Hitschfeld and Bordan (1954), 1) a PIA of about 10 dB should be considered as the upper limit a standard algorithm based on this solution is able to correct and 2) optimization of one parameter is absolutely necessary to obtain reliable corrections. This optimization requires additional measurements such as rain gauge data, as suggested by Hitschfeld and Bordan themselves, or PIA estimates provided by mountain returns or by receiving antennas (Delrieu et al. 1999b; Serrar et al. 2000).

For X band, Figs. 8–10 yield maximum ranges between 16 and 20 km if one accepts PIAs greater than 10 dB for about 1% of the rainy weather duration. This result is compatible with the idea of using X-band radars for local hydrometeorological surveillance in urban and/or mountainous regions in complement to S- or C-band conventional weather radar networks (Delrieu et al. 1997). It should be kept in mind that the highest attenuation cases also correspond to the most critical periods in terms of water management, however. The development of stable correction schemes for high attenuation therefore remains an important objective for the ''promoters'' of this concept. The use of the algorithm proposed by Marzoug and Amayenc (1994) that makes a direct use of PIA measurements for each ray is certainly one of these solutions for the specific measurement configurations in which a mountain belt surrounds the area of interest. Such configurations are not so uncommon in the mountainous regions of southern Europe.

Within the 60-km range, the probability of having 10-dB attenuation effects at C band can be estimated from the current study to about 0.1%. It may be concluded that C-band attenuation is worth being corrected [recall that 10 dB is a factor of about 5 on the rain-rate scale according to Eqn. (14)] and may be correctable with a standard algorithm. We point out again, however, the need to optimize parameterization of the attenuation scheme with additional information (PIA measurements for instance). Furthermore, because the hypotheses usually required for such attenuation correction schemes [namely, 1) DSD homogeneity, and 2) uniform beam filling] are likely to be satisfied only over short ranges, C-band attenuation may, in fact, be very difficult to cope with. As an alternative to standard schemes based on reflectivity data only, polarimetric techniques offer interesting perspectives for improved rain estimation at attenuating wavelengths (e.g., Sauvageot 1996; Testud et al. 2000).

Acknowledgments. The authors thank Remko Uijlenhoet for his constructive comments about this work. The current study was performed under the HYDROMET

project funded by the Environment and Climate Program of the European Community (Grant ENV4CT96-0290).

REFERENCES

Andrieu, H., and J. D. Creutin, 1995: Identification of vertical profiles of radar reflectivities for hydrological applications using an inverse method. Part I: Formulation. *J. Appl. Meteor.,* **34,** 225–239.

——, G. Delrieu, and J. D. Creutin, 1995: Identification of vertical profiles of radar reflectivities for hydrological applications using an inverse method. Part II: Sensitivity analysis and case study. *J. Appl. Meteor.,* **34,** 240–259.

——, J. D. Creutin, G. Delrieu, and D. Faure, 1997: Use of a weather radar for the hydrology of a mountainous area. Part 1: Radar measurement interpretation. *J. Hydrol.,* **193,** 1–25.

Beard, K. V., 1976: Terminal velocity and shape of cloud and precipitation drops aloft. *J. Atmos. Sci.,* **33,** 851–864.

Bennett, J. A., D. J. Fang, and R. C. Boston, 1984: The relationship between N_0 and Λ for Marshall–Palmer type raindrop-size distributions. *J. Climate Appl. Meteor.,* **23,** 768–771.

Boithias, L., 1984: *Propagation des Ondes Radioélectriques dans L'environnement Terrestre.* Dunod, 310 pp.

Collier, C. G., 1989: *Applications of Weather Radar Systems.* Ellis Horwood, 294 pp.

Creutin, J. D., D. Faure, and H. Andrieu, 1997: Use of a weather radar for the hydrology of a mountainous area. Part II: Validation of radar measurement. *J. Hydrol.,* **193,** 26–44.

Delrieu, G., J. D. Creutin, and I. Saint-André, 1991: Mean *K–R* relationships: Practical results for typical weather radar wavelengths. *J. Atmos. Oceanic Technol.,* **8,** 467–476.

——, S. Caoudal, and J. D. Creutin, 1997: Feasibility of using mountain return for the correction of ground-based X-band weather radar. *J. Atmos. Oceanic Technol.,* **14,** 368–385.

——, L. Hucke, and J. D. Creutin, 1999a: Attenuation in rain for X- and C-band weather radar systems: Sensitivity with respect to the drop size distribution. *J. Appl. Meteor.,* **38,** 57–68.

——, S. Serrar, E. Guardo, and J. D. Creutin, 1999b: Rain measurement in hilly terrain with X-band radar systems: Accuracy of path-integrated attenuation estimates derived from mountain returns. *J. Atmos. Oceanic Technol.,* **16,** 405–416.

Doviak, R. J., and D. S. Zrnić, 1993: *Doppler Radar and Weather Observations.* 2d ed. Academic Press, 562 pp.

Hildebrand, P. H., and R. K. Moore, 1990: Meteorological radar observations from mobile platforms. *Radar in Meteorology: Battan Memorial and 40th Anniversary Radar Meteorology Conference,* D. Atlas, Ed., Amer. Meteor. Soc., 287–314.

Hitschfeld, W., and J. Bordan, 1954: Errors inherent in the radar measurement of rainfall at attenuating wavelengths. *J. Meteor.,* **11,** 58–67.

Joss, J., and A. Waldvogel, 1969: Raindrop size distribution and sampling size error. *J. Atmos. Sci.,* **26,** 566–569.

——, and ——, 1990: Precipitation measurement and hydrology. *Radar in Meteorology: Battan Memorial and 40th Anniversary Radar Meteorology Conference,* D. Atlas, Ed., Amer. Meteor. Soc., 577–606.

Marshall, J. S., and W. K. Palmer, 1948: The distribution of raindrops with size. *J. Meteor.,* **5,** 165–166.

Marzoug, M., and P. Amayenc, 1994: A class of single- and dual-frequency algorithms for rain-rate profiling from a spaceborne radar. Part I: Principle and tests from numerical simulations. *J. Atmos. Oceanic Technol.,* **11,** 1480–1506.

Sauvageot, H., 1992: *Radarmeteorology.* Artech House, 366 pp.

——, 1996: Polarimetric radar at attenuated wavelengths as a hydrological sensor. *J. Atmos. Oceanic Technol.,* **13,** 630–637.

Serrar, S., G. Delrieu, J. D. Creutin, and R. Uijlenhoet, 2000: Mountain reference technique: Use of mountain returns to calibrate weather radars operating at attenuating wavelengths. *J. Geophys. Res.,* **105,** 2281–2290.

Smith, P. L., 1986: On the sensitivity of weather radars. *J. Atmos. and Oceanic Technol.,* **3,** 704–713.

Smyth, T. J., and A. J. Illingworth, 1997: Correction for severe attenuation at S-band. Preprints, *28th Conf. on Radar Meteorology,* Austin, TX, Amer. Meteor. Soc., 7–8.

Testud, J., E. Le Bouar, E. Obligis, and M. Ali-Mehenni, 2000: The rain profiling algorithm applied to polarimetric weather radar. *J. Atmos. Oceanic Technol.,* **17,** 332–356.

Tourasse, P., 1981: Analyses spatiales et temporelles de précipitations et utilisation opérationnelle dans un système de prévision des crues. Application aux régions cévenoles. Ph.D. dissertation, Universities of Grenoble (UJF, INPG), 189 pp.

Weible, M. L., and D. Sirmans, 1976: Simulation of attenuation by rainfall at a wavelength of 5 cm. Preprints, *17th Conf. on Radar Meteorology,* Seattle, WA, Amer. Meteor. Soc., 75–78.